

Distinguishing thermal versus quantum annealing using probability-flux signatures across interaction networks

Yoshiaki Horiike  ^{a)} and Yuki Kawaguchi  ^{1,2}

¹⁾Department of Applied Physics, Nagoya University, Nagoya, Japan

²⁾Research Center for Crystalline Materials Engineering, Nagoya University, Nagoya, Japan

(Dated: 20 November 2025)

Simulated annealing¹ provides a heuristic solution to combinatorial optimization problems². The cost function of a problem is mapped to the energy function of a physical many-body system, and, using thermal¹ or quantum^{3–7} fluctuations, the system explores the state space to find the ground state, which may correspond to the optimal solution of the problem. Studies have highlighted both the similarities^{8–10} and differences^{11–14} between thermal and quantum fluctuations. Nevertheless, fundamental understanding of thermal and quantum annealing remains incomplete, making it difficult to design problem instances that fairly compare the two methods^{15–18}. Here, we investigate the many-body dynamics of thermal and quantum annealing by examining all possible interaction networks of $\pm J$ Ising spin systems up to seven spins. Our comprehensive investigation reveals that differences between thermal and quantum annealing emerge for particular interaction networks, indicating that the structure of the energy landscape distinguishes the two dynamics. We identify the microscopic origin of these differences through probability fluxes in state space, finding that the two dynamics are broadly similar but that quantum tunnelling produces qualitative differences. Our results provide insight into how thermal and quantum fluctuations navigate a system toward the ground state in simulated annealing, and are experimentally verifiable in atomic, molecular, and optical systems^{19,20}. Furthermore, these insights may improve mappings of optimization problems to Ising spin systems, yielding more accurate solutions in faster simulated annealing and thus benefiting real-world applications in industry²¹. Our comprehensive survey of interaction networks and visualization of probability flux can help to understand, predict, and control quantum advantage in quantum annealing^{22,23}.

INTRODUCTION

Combinatorial optimization problems² are real-life problems, and in practice the exact solution is often intractable because of the combinatorial explosion of the search space. The problem is formulated as the minimization (or maximization) of a multivariate cost function under the constraints, and the cost function often has many local minima (or maxima). Simulated annealing¹ is general method to obtain the (heuristic) solution to combinatorial optimization problems. Inspired by physics, the method map the problem into physical system and, employs the fluctuations to explore the search space: initially the fluctuation is the strongest and the (physical) system explores the search (or state) space irrelevant to cost (or energy), and then the fluctuation is gradually reduced so that the system settles into the lowest-cost (or ground) states. By changing the strength of fluctuation, the system is expected to escape from the local minima, which corresponds to the undesired solutions.

There are two types—thermal and quantum—of fluctuations in simulated annealing. We use the terminology, thermal annealing¹ (TA) and quantum annealing^{3–7} (QA), depending on the type of fluctuation we employ. Studies^{8–10} have shown that the quantum fluctuations play the similar role as thermal one^{8,24}. Nevertheless, the energy landscape picture recall the vivid difference between the dynamics of those two fluctuations^{11–14}: the thermal fluctuation lead the system to jump over to the energy barriers, but quantum fluctuation allow the system to tunnel through energy barriers. Results from experimental studies^{25–27} indeed support quantum tunnelling effect in disordered magnet. The similarity and difference between the thermal and quantum fluctuation are still under investigation.

With the hope to outperform TA²³ and to achieve quantum speed up²² in solving optimization problems, QA as well as adiabatic (or diabatic) quantum computing²⁸ has been studied over the last decades^{12–14,21–23,29–31}, but the superiority of QA

over TA is still under debate^{22,23}. Theoretically, fluctuation-reduction rate of QA can be faster^{9,24,32–34} than that of TA³⁵ to have adiabatic time evolution, i.e., QA is allowed to reduce the fluctuation faster than TA while keeping the system in the instantaneous ground state. Several theoretical and numerical studies, such as refs.^{7,36–43}, indeed show that the QA outperforms TA for certain problem instances. Other theoretical and numerical studies, such as refs.^{7,15,41,44–46}, however, show that the QA cannot exhibit its advantage for particular problem instances. Even with the development of the QA devices⁴⁷, the experimental results are assorted with supporting and opposing evidence of quantum advantages; see, for example, refs.^{17,22,47–70}. Those arise from the lack of fundamental understanding of difference between thermal and quantum fluctuation.

The difficulty to compare the performance of TA and QA arises not only from problem instances (or benchmark problems)^{15–18} and annealing schedules but also arbitrary parameters for numerical simulation⁴⁵. Although the performance for specific tasks, i.e., benchmark problems, is one of the metrics to compare TA and QA²³, there is no standard guiding principle to design the benchmark problems. Analytical works derive the annealing schedule to achieve the adiabatic time evolution but in practice faster schedule is chosen. There are several ways to numerically simulate QA for large system, but care must be taken to conclude the performance of QA. Those concerns lead us to the following questions: What kind of problems does QA favour? What can be said certain from the numerical simulation of TA and QA?

Here, through a lens of many-body dynamics on energy landscape^{71,72}, we show the difference between TA and QA arising from interaction networks. We investigate the annealing dynamics of TA and QA by examining $\pm J$ Ising spin systems on all possible interaction networks up to seven spins. Following the pioneering work by Kadowaki and Nishimori⁸ on QA, we compare the performance of TA and QA for comprehensive problem instances (i.e., interaction networks of $\pm J$ model) with different annealing schedules by numerically integrating the master equation and the Schrödinger equation. Our investigation reveal the follows: (1) For ferromagnetic interaction networks, QA has higher performance than TA as the inter-

^{a)}Contact author: yoshi.h@nagoya-u.jp

action network becomes sparser or denser depending on the external longitudinal field strength. (2) Probable pathway of state transitions in TA and QA are largely similar but reflect the difference between thermal and quantum fluctuations. (3) The non-monotonic time evolution of success rate in QA indicates the tunnelling between the ground state and single-spin flipped states from it. (4) For $\pm J$ interaction networks, our performance of QA over TA is not necessarily related to the number of nonzero interaction of interaction networks. (5) The probable pathways of state transitions in TA and QA for $\pm J$ interaction networks have similar trend to that of ferromagnetic interaction networks. With the probability flux, we reveal the fundamental difference between the thermal and quantum fluctuations.

NETWORK STRUCTURE AND ANNEALING DYNAMICS

Based on the comprehensively generated interaction networks, we create transition rate matrices for TA and Hamiltonian for QA. By numerically integrating the master equation and the Schrödinger equation with time-dependent temperature and transverse field strength, we investigate the dynamics of TA and QA on various interaction networks. See [Generation of all possible interaction networks](#) and [Ising spin system and annealing dynamics](#) in [Methods](#) for details of generating interaction networks and the dynamics of TA and QA.

FERROMAGNETIC ISING SPIN SYSTEMS

We first consider how the interaction network structure affects the success rate of TA and QA for ferromagnetic Ising spin systems. We limit our investigation to all possible $+J$ Ising spin systems, where the ground state is trivially known as the all-up or all-down state. Although the ground state is trivial, the energy landscape and the dynamics of TA and QA depend on the interaction network structure, and we can systematically investigate the effect of interaction network structure.

In Fig. 1a, we show all possible five-spin interaction networks. We show the time evolution of the success rate, i.e., the probability of finding the system in the ground state, for each interaction network in Fig. 1b. To avoid the two degenerate ground states due to \mathbb{Z}_2 symmetry, we apply a small longitudinal field $h_i = 0.5J/N$ for all i , thus the system approach to the all-spin-up state and all-spin-down state is the first excited state. Here, $N = 5$ is the system size and nonzero interaction strength is given as J/N to normalize the total interaction strength. Figure 1b shows that the QA success rate is relatively network independent and closely following the adiabatic limit. Contrary to the QA, the success rate of TA depends on the interaction network structure and as the interaction network become denser, i.e., number of non-zero interaction increase, the success rate of TA decrease and deviate from its adiabatic limit. Thus, for TA, finding the ground state becomes more non-trivial as the number of nonzero interaction increases.

To validate our findings above, we investigate the success rate difference between TA and QA and difference of their adiabatic limits for all possible interaction networks up to seven spins. Figure 2 shows the success rate difference between TA and QA at the end of annealing process, i.e., $p_{QA}(\infty) - p_{TA}(\infty)$, and the difference between their adiabatic limits, i.e., $p_{AQA}(\infty) - p_{QA}(\infty)$, and $p_{ATA}(\infty) - p_{TA}(\infty)$. Our results confirm that QA has typically higher success rate than TA for denser interaction networks for some range of strength of external longitudinal field. In the limit of strong longitudinal field, the problem is trivial as the longitudinal field dominates the interaction and

interaction network structure becomes irrelevant. In the limit of weak longitudinal field, the problem is difficult as the two trivial ground states are weakly distinguishable. In between those two limits, QA outperforms TA for denser interaction networks for relatively stronger longitudinal field, but as the longitudinal field becomes weaker QA outperforms TA for rather sparse interaction networks. Our results indicate that the interaction network structure affects the performance of TA and QA, but it has non-trivial dependency on the strength of longitudinal field.

We also investigate how TA and QA deviate from their adiabatic limits. In parameter range of QA outperforming TA, both TA and QA are slightly deviate from their adiabatic limits. Thus, the time evolution of both TA and QA are not fully adiabatic, but both dynamics are close to the adiabatic limit. The difference between TA and QA is that their deviation from the adiabatic limit behave differently with the strength of longitudinal field. For QA, as the longitudinal field becomes stronger, the deviation become smaller, but for TA, it becomes larger and then smaller. Such difference indicates the different nature of thermal and quantum annealing dynamics.

So far we have investigated the success rate of TA and QA. To further understand the difference between TA and QA, we analyse the microscopic dynamics of both annealing methods by examining the probability flux between states. Probability flux characterizes the time evolution of the probability distribution, and by visualizing them we can understand how the system explores the state space. We use the difference between the forward and backward joint transition rate for TA and QA. See [Thermal and quantum probability flux](#) in [Methods](#) for details.

In Fig. 3, we show the time-integrated probability fluxes, i.e., the total amount of flux streamed during the process. Overall, the pathways of state transitions in TA and QA are similar as shown in Fig. 3a and b. The probability flux gradually accumulates as it approaches to the ground state on the right side of each diagram. There are, however, notable differences between TA and QA. In Fig. 3c, we show the difference between the time-integrated probability fluxes of TA and QA by subtracting probability flux of QA from that of TA. The difference indicates that for each network structure the pathways of state transitions in TA and QA have characteristic differences. For sparse interaction networks such as networks 5-018 and 5-066 exhibits unique state transition pathways in stronger in TA than QA. Those pathways indicate that the dynamics of TA is more constrained (highly selected order of spin flips) than that of QA, and the system may tend to be trapped in local minima. For denser interaction networks such as networks 5-458 and 5-679, the probability fluxes from the false ground state (all-spin-down state) stream toward the true ground state (all-spin-up state). Such pathway is more pronounced in QA than TA and contributes to the higher success rate of QA in denser networks.

Another aspect of the difference between TA and QA is revealed by time-dependent probability flux. Unlike Fig. 3, which shows the time-integrated probability fluxes, we then investigate the time-dependent probability fluxes. In Fig. 4, we show, for example, the time evolution of the success rate (Fig. 4a) of network 5-219, and the probability fluxes at seven time points (Fig. 4b-d). Figure 4a reveals the detailed dynamics of QA, which is the oscillatory time evolution of the success rate⁷. Such oscillatory behaviour is not observed in TA dynamics. To investigate the origin of such oscillatory behaviour, we examine the probability fluxes at each time point in the oscillatory time range. Figure 4b and c show the quantum and thermal probability fluxes at each selected time point respectively, and Fig. 4d shows the difference between them. At time t_1 , both TA

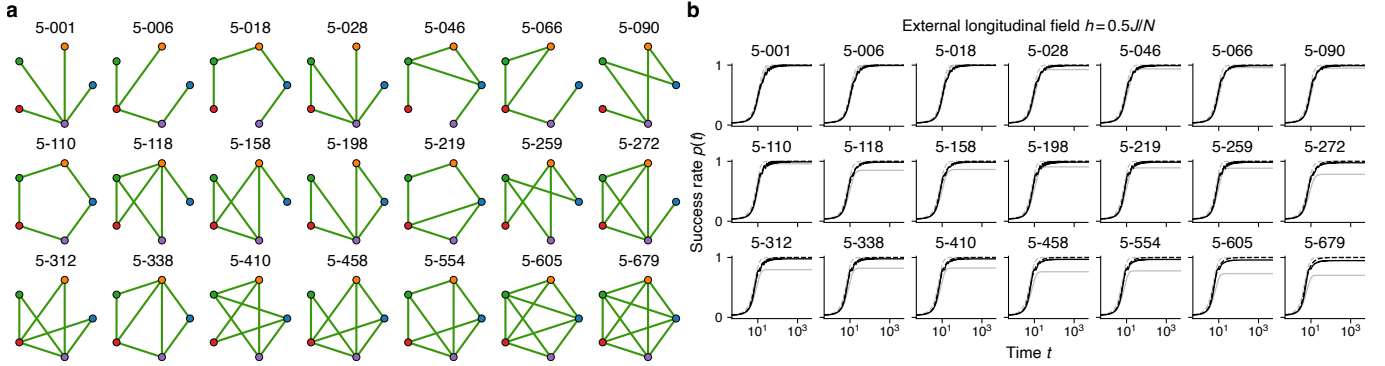


Fig. 1 | The success rate dependency on the interaction network structure. **a**, $\pm J$ five-spin interaction networks. The node represents spins and the edges represent interactions. The colour of nodes indicates the spin identifier. The solid green edges represent the ferromagnetic interaction $+J/N$, and the dashed red edges represent the antiferromagnetic interaction $-J/N$ (not shown here). Interaction network identifiers are shown on the top of each network. **b**, Time evolution of the success rate corresponding to panel **a**. The dark and light solid lines represent TA and QA results respectively, and the dark and light dashed lines represent the adiabatic limits of TA and QA respectively. External field is set to be $h_i = 0.5/J$ for all i . The reciprocal annealing schedule is used.

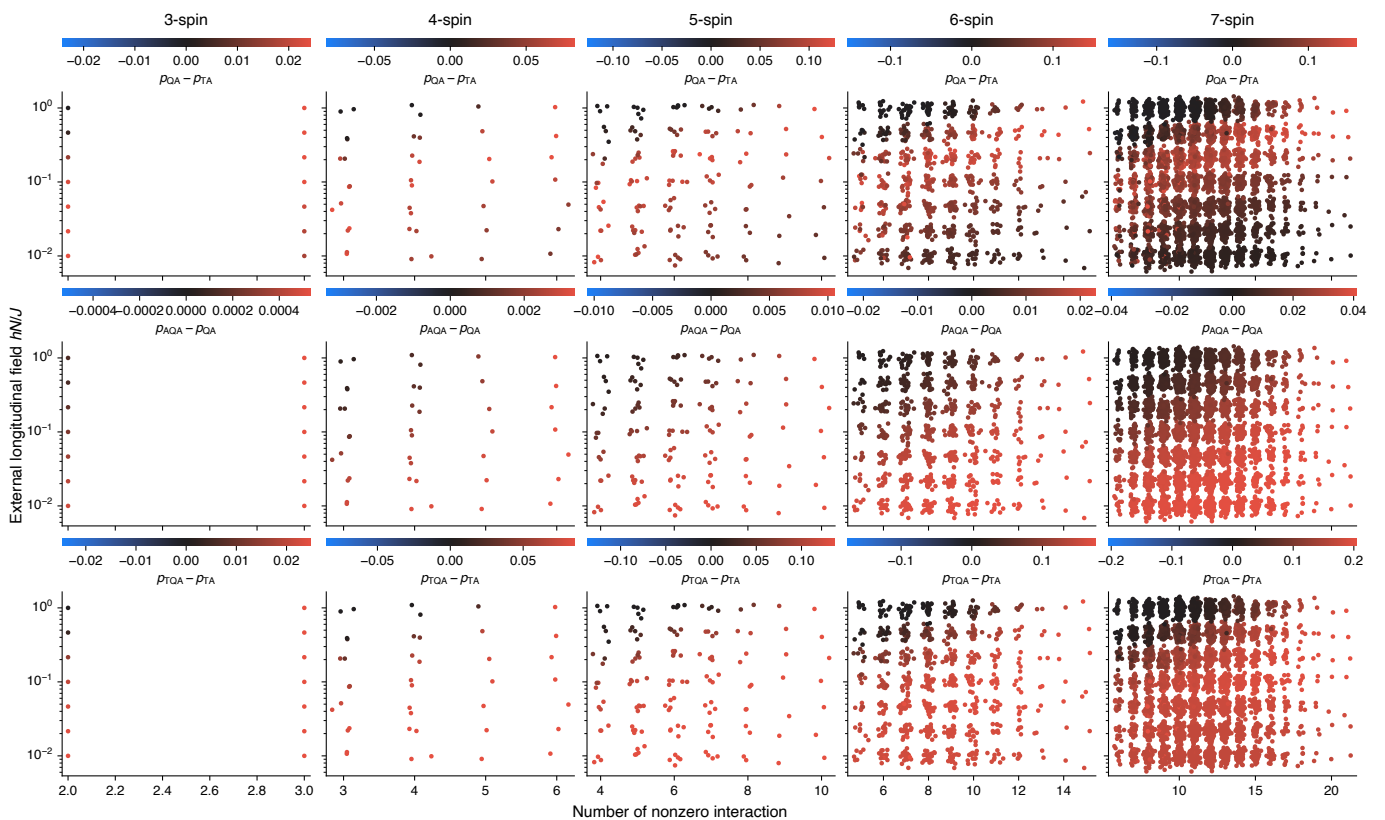


Fig. 2 | Comparing success rate difference between TA and QA. From left to right, the panels represent the results for three- to seven-spin interaction networks. From top to bottom, the panels show the results for the success rate difference between QA and TA, i.e., $p_{\text{QA}}(\infty) - p_{\text{TA}}(\infty)$, the difference between the adiabatic limits of TA and TA, i.e., $p_{\text{ATA}}(\infty) - p_{\text{TA}}(\infty)$, and the difference between the adiabatic limits of QA and QA, i.e., $p_{\text{AQA}}(\infty) - p_{\text{QA}}(\infty)$. The horizontal axis represents the number of nonzero interactions, and the vertical axis represents external longitudinal field strength. Each data point corresponds to an interaction network instance. For visualization, we add small random noise to the data points to remove the overlap of data points.

and QA exhibit similar probability fluxes though quantum ones have higher magnitude, which contribute to the higher success rate. At time t_2 , the quantum probability fluxes become weaker and even change their direction of stream: the probability tunnels back from the ground state to the single-spin flipped states from it while the thermal probability fluxes still stream toward the ground state. This backward tunnelling is the origin of the oscillatory behaviour of success rate of QA.

$\pm J$ ISING SPIN SYSTEMS

The findings above indicate that the interaction network structure indeed affects the dynamics of TA and QA. The success rate difference between TA and QA for ferromagnetic interacting system roughly depend on the number of nonzero interactions, and the probable pathways of state transitions in TA and QA are largely similar but exhibit the difference due to tunnelling. How are those findings valid for more general interaction networks, particularly those with geometric frustration? To answer the question, we investigate the dynamics of TA and QA for $\pm J$

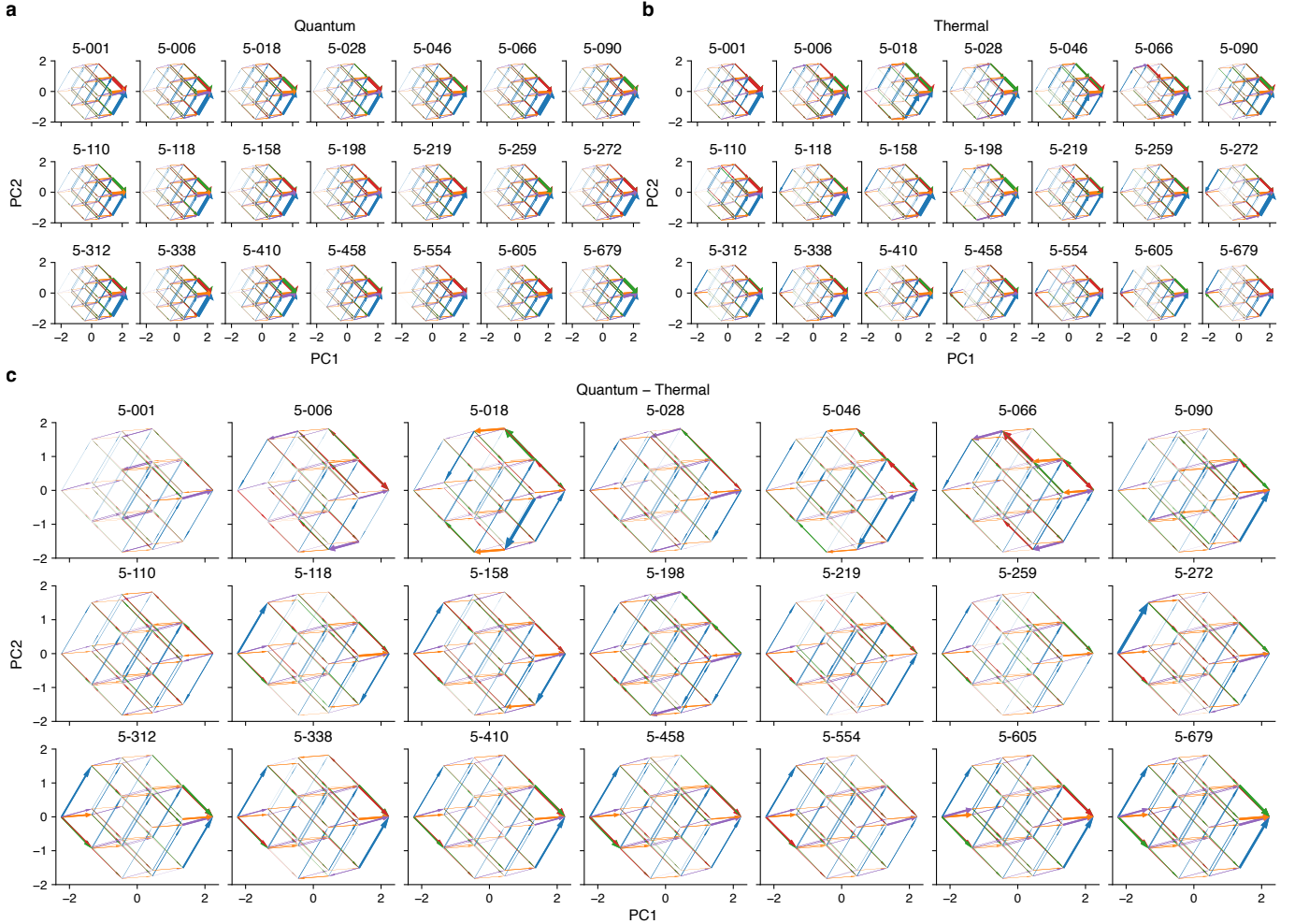


Fig. 3 | Time-integrated probability fluxes of TA and QA. **a**, Time-integrated quantum probability fluxes $\{\Delta\mathcal{J}_Q(s, s')\}$. **b**, Time-integrated thermal probability fluxes $\{\Delta\mathcal{J}_T(s, s')\}$. **c**, Difference between quantum and thermal probability fluxes, $\{\Delta\mathcal{J}_Q(s, s') - \Delta\mathcal{J}_T(s, s')\}$. Each arrow represents the time-integrated thermal probability flux, and its width is proportional to the magnitude of the flux $|\Delta\mathcal{J}(s, s')|$, and direction corresponds to the sign of the flux $\text{sgn}(\Delta\mathcal{J}(s, s'))$. The colour of each arrow indicates the spin identifier of the flipped spin, cf. Fig. 1a.

Ising spin systems on all possible interaction networks with four spins.

In Fig. 5, we show all possible four-spin $\pm J$ interaction networks (Fig. 5a) and corresponding time evolution of the success rate (Fig. 5b). External field is set to be $\mathbf{h} = 0.4J/Ns_g$ for all interaction networks, where s_g is the ground state of each interaction network: we navigate the system toward the single ground state by applying the longitudinal field. Note that the some of interaction networks have more than two ground states due to frustration, and we mark such networks with star symbol in Fig. 5. As the external field for such intrinsically degenerate systems, we still choose one of the ground states to define the longitudinal field, and success rate is defined as the sum of the probabilities of all ground states.

We find, in Figure 5b, that the QA closely follows its adiabatic limit but the TA deviates from its adiabatic limit for some interaction networks: this is similar to the findings for ferromagnetic interaction networks. Nevertheless, the success rate difference between TA and QA does not necessarily depend on the number of nonzero interactions unlike the findings for ferromagnetic interaction networks. In some dense interaction networks such as networks 4-31, 4-33, 4-34, 4-35, 4-36, 4-38, 4-40, and 4-42, the difference between TA and QA is negligible. Those interaction networks have frustrated loop in network structure, which alter the energy landscape and the dynamics of TA and QA. Thus, the energy landscape changed by frustration affect the performance of TA and QA in non-trivial manner.

To further understand the difference between TA and QA for $\pm J$ Ising spin systems, we investigate the microscopic dynamics by examining the time-integrated probability fluxes. In Fig. 6, we show the quantum and thermal time-integrated probability fluxes and difference between them for four-spin $\pm J$ interaction networks. Again the overall pathways of state transitions in TA and QA are similar as shown in Fig. 6a and b. The difference between them shown in Fig. 6c indicates that the characteristic differences in the pathways of state transitions. As we have seen in ferromagnetic interaction networks, as the interaction network becomes denser, the quantum probability flux from the false ground state streams toward the true ground state more than the thermal one. Nevertheless, as expected from the results of Fig. 5, Some interaction networks such as networks 4-30, 4-31, 4-33, 4-34, 4-35, 4-36, 4-38, 4-40, and 4-42 exhibit the strong thermal fluctuation than the thermal one. Although the success rate of most of these networks are similar between TA and QA (Fig. 5b), thermal time-integrated probability fluxes are stronger than quantum ones. We anticipate that such difference arise from the oscillatory tunnelling behaviour as we have seen in Fig. 4. Because the time-integrated probability fluxes ignore such oscillatory behaviour, the probability flux between TA and QA differ but the success rate does not.

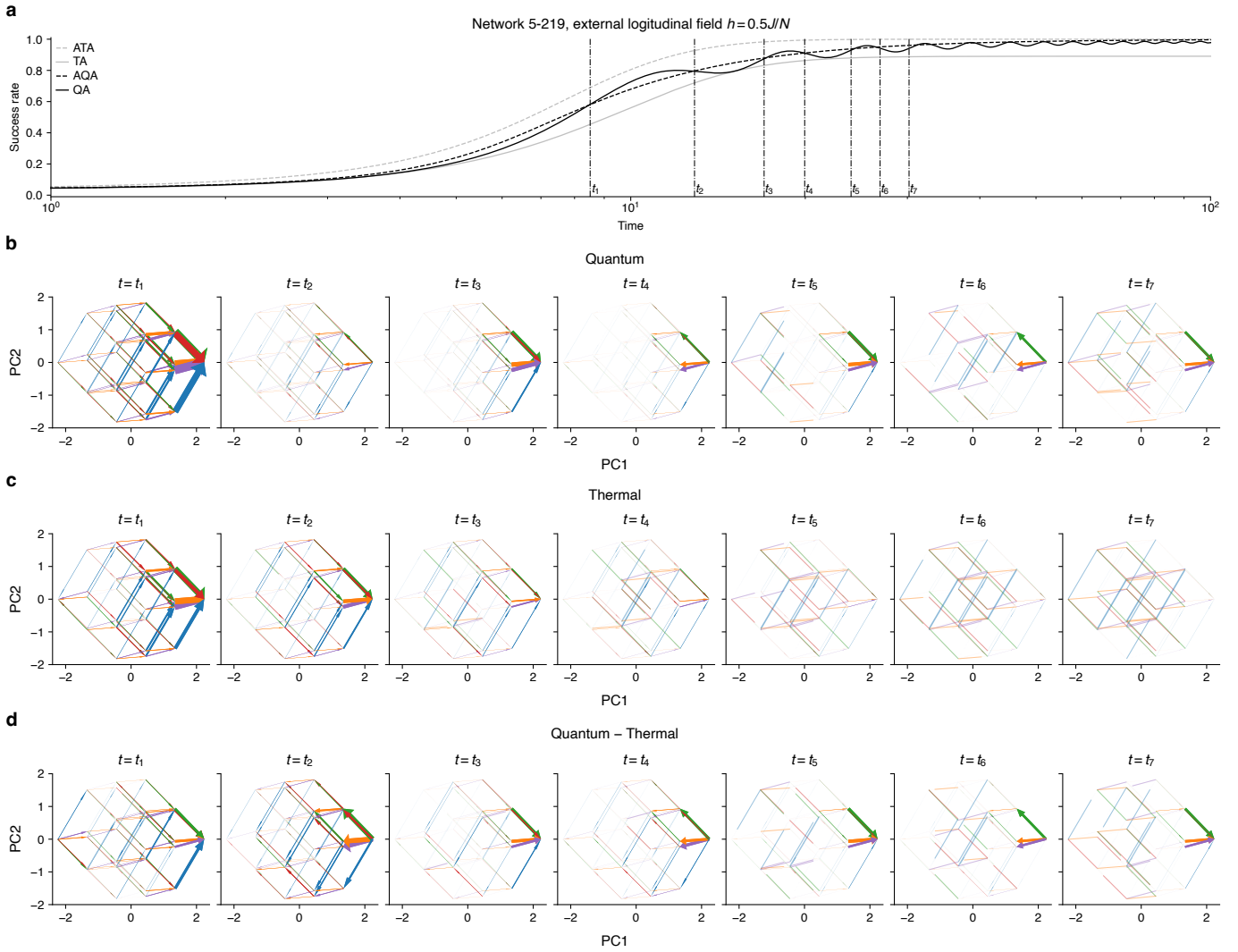


Fig. 4 | Probability fluxes difference between TA and QA. **a**, Time evolution of success rate of network 5-219. We select seven time points to investigate the time-dependency of probability flux. This panel is magnified version of corresponding panel in Fig. 1**b**. **b**, Quantum probability fluxes at each time point. **c**, Thermal probability fluxes at each time point. **d**, Difference between quantum and thermal probability fluxes at each time point. For **b–d**, the arrow indicates the same as Fig. 3**a–c** but for probability flux at each time point $\mathcal{J}(s, s'; t)$.

CONCLUSION

With thermal or quantum fluctuation, simulated annealing provide heuristic solutions to combinatorial optimization problems. Quantum mechanical phenomena are expected to enhance the performance of simulated annealing, but theoretical, numerical, and experimental evidence are assorted with supporting and opposing ones. Such situation arises from various factors, such as problem instances, annealing schedules, and numerical methods. In this study, we compare the dynamics of TA and QA solving ground state of $\pm J$ Ising spin systems on all possible interaction networks up to seven spins. Our comprehensive investigation reveals that the difference between TA and QA arises from the interaction network structure. With the probability flux diagram, we reveal the microscopic origin of the difference between TA and QA. Those are non-trivial pathways of state transitions and their change by frustration in interaction network structure.

Although we have demonstrated that the difference between TA and QA arise from interaction network structure of Ising spin system, our results are limited to small systems up to seven spins. Studies^{18,73} show that interaction network structure dependency of the QA dynamics of large systems, but further theoretical and numerical investigation is needed to generalize our findings to large systems. Recent atomic, molecular, and

optical physics experiments enable one to implement arbitrary interaction network of both classical and quantum Ising spin systems^{19,20,74}. Simulated annealing has been executed in various platforms such as trapped ions^{75,76}, parametric oscillators^{77–86}, atoms in cavity^{87–89}, Rydberg atoms⁹⁰, and quantum wire⁹¹. Experiments with those platforms may validate our findings and further explore the difference between TA and QA.

Our findings may provide guiding principles to design problem instances in real-life problem. The results indicate the condition on the problem instance to extract the thermal or quantum advantages in simulated annealing. By improving the mapping of optimization problem to the Ising spin system⁹², one may achieve more accurate solutions in faster simulated annealing, which are beneficial in broad range of industrial applications^{21,31} such as machine learning⁹³, pharmaceutics⁹⁴, and transportation⁹⁵.

From the viewpoint of quantum advantages, our results provide insight into how thermal and quantum fluctuations navigate the system into the ground state in simulated annealing. The probability flux visualization reveals the microscopic dynamics of TA and QA on energy landscape. Such insight might lead further understanding, prediction and control of quantum advantage in quantum annealing^{22,23}.

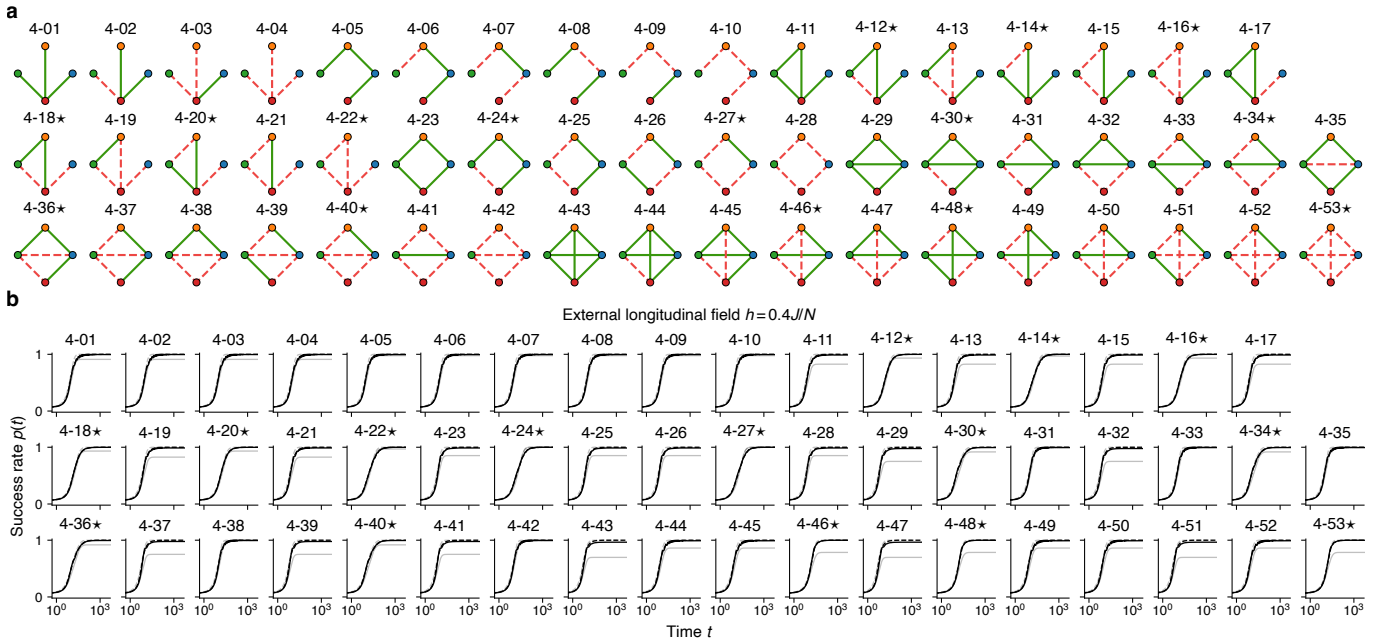


Fig. 5 | $\pm J$ four-spin interaction networks and their success rate in TA and QA. **a**, $\pm J$ four-spin interaction networks. **b**, Time evolution of the success rate corresponding to panel **a**. External field is set to be $h = 0.4J/Ns_g$ for all interaction networks, where s_g is the ground state of each interaction network. The reciprocal annealing schedule is used. See also the caption of Fig. 1a–b.

- ¹S. Kirkpatrick, C. D. Gelatt, and M. P. Vecchi, “Optimization by Simulated Annealing,” *Science* **220**, 671–680 (1983).
- ²B. Korte and J. Vygen, *Combinatorial Optimization: Theory and Algorithms*, Algorithms and Combinatorics, Vol. 21 (Springer Berlin Heidelberg, 2012).
- ³B. Apolloni, C. Carvalho, and D. De Falco, “Quantum stochastic optimization,” *Stochastic Processes and their Applications* **33**, 233–244 (1989).
- ⁴R. L. Somorjai, “Novel approach for computing the global minimum of proteins. 1. General concepts, methods, and approximations,” *J. Phys. Chem.* **95**, 4141–4146 (1991).
- ⁵P. Amara, D. Hsu, and J. E. Straub, “Global energy minimum searches using an approximate solution of the imaginary time Schrödinger equation,” *J. Phys. Chem.* **97**, 6715–6721 (1993).
- ⁶A. Finnila, M. Gomez, C. Sebenik, C. Stenson, and J. Doll, “Quantum annealing: A new method for minimizing multidimensional functions,” *Chemical Physics Letters* **219**, 343–348 (1994).
- ⁷T. Kadowaki and H. Nishimori, “Quantum annealing in the transverse Ising model,” *Phys. Rev. E* **58**, 5355–5363 (1998).
- ⁸H. Nishimori and Y. Nonomura, “Quantum Effects in Neural Networks,” *J. Phys. Soc. Jpn.* **65**, 3780–3796 (1996).
- ⁹R. D. Somma, C. D. Batista, and G. Ortiz, “Quantum Approach to Classical Statistical Mechanics,” *Phys. Rev. Lett.* **99**, 030603 (2007).
- ¹⁰H. Nishimori, J. Tsuda, and S. Knyshev, “Comparative study of the performance of quantum annealing and simulated annealing,” *Phys. Rev. E* **91**, 012104 (2015).
- ¹¹P. Ray, B. K. Chakrabarti, and A. Chakrabarti, “Sherrington-Kirkpatrick model in a transverse field: Absence of replica symmetry breaking due to quantum fluctuations,” *Phys. Rev. B* **39**, 11828–11832 (1989).
- ¹²G. E. Santoro and E. Tosatti, “Optimization using quantum mechanics: Quantum annealing through adiabatic evolution,” *J. Phys. A: Math. Gen.* **39**, R393–R431 (2006).
- ¹³A. Das and B. K. Chakrabarti, “Colloquium : Quantum annealing and analog quantum computation,” *Rev. Mod. Phys.* **80**, 1061–1081 (2008).
- ¹⁴A. Rajak, S. Suzuki, A. Dutta, and B. K. Chakrabarti, “Quantum annealing: An overview,” *Phil. Trans. R. Soc. A* **381**, 20210417 (2023).
- ¹⁵B. Altshuler, H. Krovi, and J. Roland, “Anderson localization makes adiabatic quantum optimization fail,” *Proc. Natl. Acad. Sci. U.S.A.* **107**, 12446–12450 (2010).
- ¹⁶V. Choi, “Different adiabatic quantum optimization algorithms for the NP-complete exact cover problem,” *Proc. Natl. Acad. Sci. U.S.A.* **108**, E19–E20 (2011).
- ¹⁷H. G. Katzgraber, F. Hamze, and R. S. Andrist, “Glassy Chimeras Could Be Blind to Quantum Speedup: Designing Better Benchmarks for Quantum Annealing Machines,” *Phys. Rev. X* **4**, 021008 (2014).
- ¹⁸A. D. King, E. Hoskinson, T. Lanting, E. Andriyash, and M. H. Amin, “Degeneracy, degree, and heavy tails in quantum annealing,” *Phys. Rev. A* **93**, 052320 (2016).
- ¹⁹W. Lechner, P. Hauke, and P. Zoller, “A quantum annealing architecture with all-to-all connectivity from local interactions,” *Sci. Adv.* **1**, e1500838 (2015).
- ²⁰P. Hauke, L. Bonnes, M. Heyl, and W. Lechner, “Probing entanglement in adiabatic quantum optimization with trapped ions,” *Front. Phys.* **3** (2015), 10.3389/fphy.2015.00021.
- ²¹S. Yarkoni, E. Rapponi, T. Bäck, and S. Schmitt, “Quantum annealing for industry applications: Introduction and review,” *Rep. Prog. Phys.* **85**, 104001 (2022).
- ²²T. Albash and D. A. Lidar, “Adiabatic quantum computation,” *Rev. Mod. Phys.* **90**, 015002 (2018).
- ²³P. Hauke, H. G. Katzgraber, W. Lechner, H. Nishimori, and W. D. Oliver, “Perspectives of quantum annealing: Methods and implementations,” *Rep. Prog. Phys.* **83**, 054401 (2020).
- ²⁴S. Morita and H. Nishimori, “Mathematical foundation of quantum annealing,” *J. Math. Phys.* **49**, 125210 (2008).
- ²⁵W. Wu, B. Ellman, T. Rosenbaum, G. Aeppli, and D. Reich, “From classical to quantum glass,” *Phys. Rev. Lett.* **67**, 2076–2079 (1991).
- ²⁶J. Brooke, D. Bitko, T. F. Rosenbaum, and G. Aeppli, “Quantum Annealing of a Disordered Magnet,” *Science* **284**, 779–781 (1999).
- ²⁷C. Ancona-Torres, D. M. Silevitch, G. Aeppli, and T. F. Rosenbaum, “Quantum and Classical Glass Transitions in LiHo x Y 1 - x F 4 ,” *Phys. Rev. Lett.* **101**, 057201 (2008).
- ²⁸E. Farhi, J. Goldstone, S. Gutmann, J. Lapan, A. Lundgren, and D. Preda, “A Quantum Adiabatic Evolution Algorithm Applied to Random Instances of an NP-Complete Problem,” *Science* **292**, 472–475 (2001).
- ²⁹S. Tanaka, R. Tamura, and B. K. Chakrabarti, *Quantum Spin Glasses, Annealing and Computation* (Cambridge university press, 2017).
- ³⁰E. J. Crosson and D. A. Lidar, “Prospects for quantum enhancement with diabatic quantum annealing,” *Nat Rev Phys* **3**, 466–489 (2021).
- ³¹L. P. Yulianti and K. Surendro, “Implementation of Quantum Annealing: A Systematic Review,” *IEEE Access* **10**, 73156–73177 (2022).
- ³²S. Morita and H. Nishimori, “Convergence of Quantum Annealing with Real-Time Schrödinger Dynamics,” *J. Phys. Soc. Jpn.* **76**, 064002 (2007).
- ³³Y. Kimura and H. Nishimori, “Rigorous convergence condition for quantum annealing,” *J. Phys. A: Math. Theor.* **55**, 435302 (2022).
- ³⁴Y. Kimura and H. Nishimori, “Convergence condition of simulated quantum annealing for closed and open systems,” *Phys. Rev. A* **106**, 062614 (2022).
- ³⁵S. Geman and D. Geman, “Stochastic Relaxation, Gibbs Distributions, and the Bayesian Restoration of Images,” *IEEE Trans. Pattern Anal. Mach. Intell. PAMI-6*, 721–741 (1984).
- ³⁶G. E. Santoro, R. Martoňák, E. Tosatti, and R. Car, “Theory of Quantum Annealing of an Ising Spin Glass,” *Science* **295**, 2427–2430 (2002).
- ³⁷R. Martoňák, G. E. Santoro, and E. Tosatti, “Quantum annealing by the path-integral Monte Carlo method: The two-dimensional random Ising model,” *Phys. Rev. B* **66**, 094203 (2002).
- ³⁸R. D. Somma, S. Boixo, H. Barnum, and E. Knill, “Quantum Simulations of Classical Annealing Processes,” *Phys. Rev. Lett.* **101**, 130504 (2008).
- ³⁹R. D. Somma, D. Nagaj, and M. Kieferová, “Quantum Speedup by Quantum Annealing,” *Phys. Rev. Lett.* **109**, 050501 (2012).

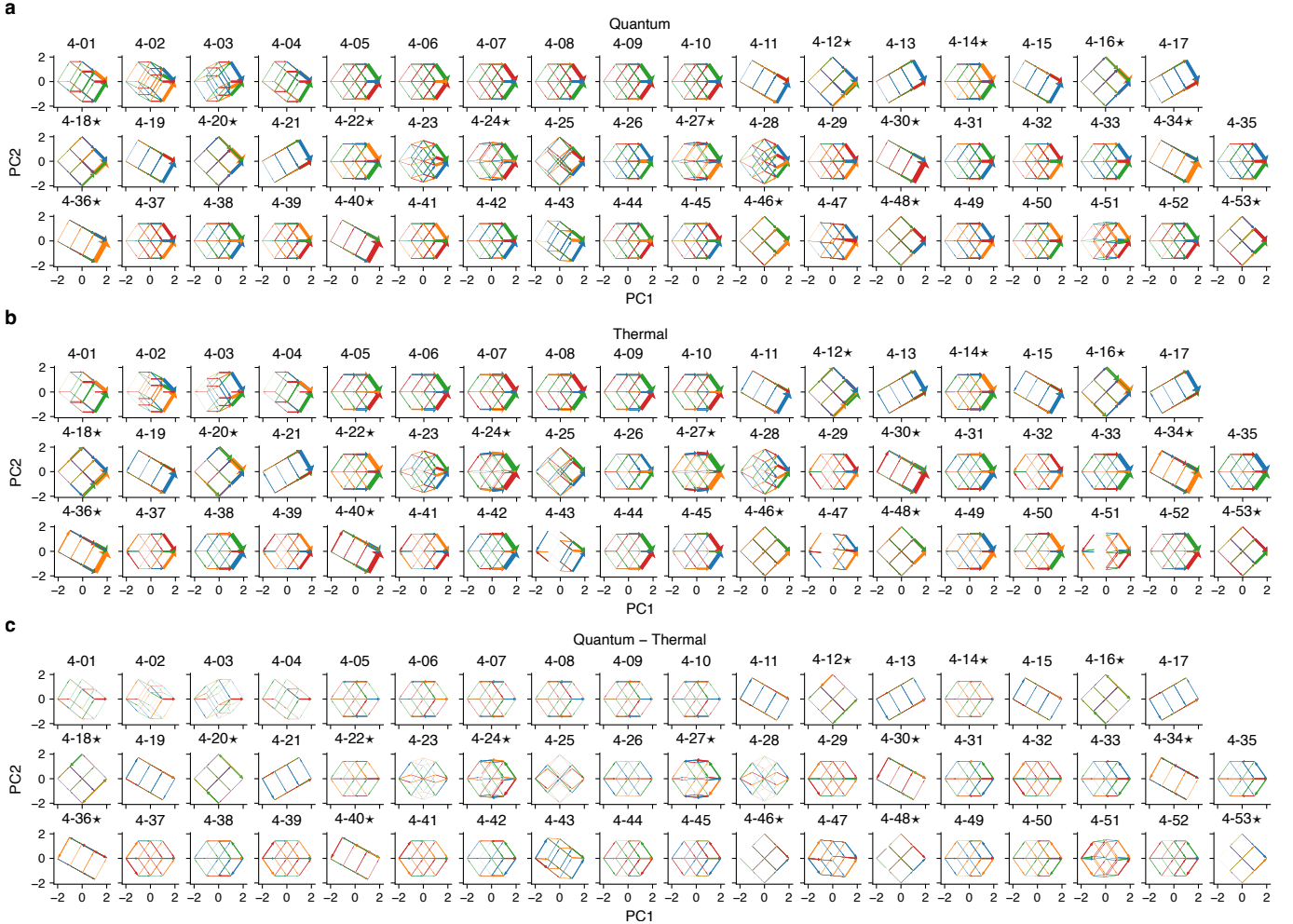


Fig. 6 | Time-integrated probability fluxes of $\pm J$ four-spin interaction networks in TA and QA. **a**, Time-integrated quantum probability fluxes. **b**, Time-integrated thermal probability fluxes. **c**, Difference between quantum and thermal probability fluxes. See the caption of Fig. 3 for details.

- ⁴⁰T. Zanca and G. E. Santoro, “Quantum annealing speedup over simulated annealing on random Ising chains,” *Phys. Rev. B* **93**, 224431 (2016).
- ⁴¹M. M. Wauters, R. Fazio, H. Nishimori, and G. E. Santoro, “Direct comparison of quantum and simulated annealing on a fully connected Ising ferromagnet,” *Phys. Rev. A* **96**, 022326 (2017).
- ⁴²C. Baldassi and R. Zecchina, “Efficiency of quantum vs. classical annealing in nonconvex learning problems,” *Proc. Natl. Acad. Sci. U.S.A.* **115**, 1457–1462 (2018).
- ⁴³E. Starchl and H. Ritsch, “Unraveling the origin of higher success probabilities in quantum annealing versus semi-classical annealing,” *J. Phys. B: At. Mol. Opt. Phys.* **55**, 025501 (2022).
- ⁴⁴Y. Matsuda, H. Nishimori, and H. G. Katzgraber, “Ground-state statistics from annealing algorithms: Quantum versus classical approaches,” *New J. Phys.* **11**, 073021 (2009).
- ⁴⁵B. Heim, T. F. Rønnow, S. V. Isakov, and M. Troyer, “Quantum versus classical annealing of Ising spin glasses,” *Science* **348**, 215–217 (2015).
- ⁴⁶C.-W. Liu, A. Polkovnikov, and A. W. Sandvik, “Quantum versus Classical Annealing: Insights from Scaling Theory and Results for Spin Glasses on 3-Regular Graphs,” *Phys. Rev. Lett.* **114**, 147203 (2015).
- ⁴⁷M. W. Johnson, M. H. S. Amin, S. Gildert, T. Lanting, F. Hamze, N. Dickson, R. Harris, A. J. Berkley, J. Johansson, P. Bunyk, E. M. Chapple, C. Enderud, J. P. Hilton, K. Karimi, E. Ladizinsky, N. Ladizinsky, T. Oh, I. Perminov, C. Rich, M. C. Thom, E. Tolkacheva, C. J. S. Truncik, S. Uchaikin, J. Wang, B. Wilson, and G. Rose, “Quantum annealing with manufactured spins,” *Nature* **473**, 194–198 (2011).
- ⁴⁸A. Perdomo-Ortiz, N. Dickson, M. Drew-Brook, G. Rose, and A. Aspuru-Guzik, “Finding low-energy conformations of lattice protein models by quantum annealing,” *Sci Rep* **2**, 571 (2012).
- ⁴⁹N. G. Dickson, M. W. Johnson, M. H. Amin, R. Harris, F. Altomare, A. J. Berkley, P. Bunyk, J. Cai, E. M. Chapple, P. Chavez, F. Cioata, T. Cirip, P. deBuen, M. Drew-Brook, C. Enderud, S. Gildert, F. Hamze, J. P. Hilton, E. Hoskinson, K. Karimi, E. Ladizinsky, N. Ladizinsky, T. Lanting, T. Mahon, R. Neufeld, T. Oh, I. Perminov, C. Petroff, A. Przybysz, C. Rich, P. Spear, A. Teaciuc, M. C. Thom, E. Tolkacheva, S. Uchaikin, J. Wang, A. B. Wilson, Z. Merali, and G. Rose, “Thermally assisted quantum annealing of a 16-qubit problem,” *Nat Commun* **4**, 1903 (2013).
- ⁵⁰S. Boixo, T. Albash, F. M. Spedalieri, N. Chancellor, and D. A. Lidar, “Experimental signature of programmable quantum annealing,” *Nat Commun* **4**, 2067 (2013).
- ⁵¹Z. Bian, F. Chudak, W. G. Macready, L. Clark, and F. Gaitan, “Experimental Determination of Ramsey Numbers,” *Phys. Rev. Lett.* **111**, 130505 (2013).
- ⁵²K. L. Pudenz, T. Albash, and D. A. Lidar, “Error-corrected quantum annealing with hundreds of qubits,” *Nat Commun* **5**, 3243 (2014).
- ⁵³J. A. Smolin and G. Smith, “Classical signature of quantum annealing,” *Front. Phys.* **2** (2014), 10.3389/fphy.2014.00052.
- ⁵⁴T. F. Rønnow, Z. Wang, J. Job, S. Boixo, S. V. Isakov, D. Wecker, J. M. Martinis, D. A. Lidar, and M. Troyer, “Defining and detecting quantum speedup,” *Science* **345**, 420–424 (2014).
- ⁵⁵S. Boixo, T. F. Rønnow, S. V. Isakov, Z. Wang, D. Wecker, D. A. Lidar, J. M. Martinis, and M. Troyer, “Evidence for quantum annealing with more than one hundred qubits,” *Nature Phys* **10**, 218–224 (2014).
- ⁵⁶T. Lanting, A. J. Przybysz, A. Yu. Smirnov, F. M. Spedalieri, M. H. Amin, A. J. Berkley, R. Harris, F. Altomare, S. Boixo, P. Bunyk, N. Dickson, C. Enderud, J. P. Hilton, E. Hoskinson, M. W. Johnson, E. Ladizinsky, N. Ladizinsky, R. Neufeld, T. Oh, I. Perminov, C. Rich, M. C. Thom, E. Tolkacheva, S. Uchaikin, A. B. Wilson, and G. Rose, “Entanglement in a Quantum Annealing Processor,” *Phys. Rev. X* **4**, 021041 (2014).
- ⁵⁷T. Albash, T. Rønnow, M. Troyer, and D. Lidar, “Reexamining classical and quantum models for the D-Wave One processor: The role of excited states and ground state degeneracy,” *Eur. Phys. J. Spec. Top.* **224**, 111–129 (2015).
- ⁵⁸T. Albash, W. Vinci, A. Mishra, P. A. Warburton, and D. A. Lidar, “Consistency tests of classical and quantum models for a quantum annealer,” *Phys. Rev. A* **91**, 042314 (2015).
- ⁵⁹H. G. Katzgraber, F. Hamze, Z. Zhu, A. J. Ochoa, and H. Munoz-Bauza, “Seeking Quantum Speedup Through Spin Glasses: The Good, the Bad, and the Ugly,” *Phys. Rev. X* **5**, 031026 (2015).

- ⁶⁰D. Venturelli, S. Mandrà, S. Knysh, B. O’Gorman, R. Biswas, and V. Smelyanskiy, “Quantum Optimization of Fully Connected Spin Glasses,” *Phys. Rev. X* **5**, 031040 (2015).
- ⁶¹I. Hen, J. Job, T. Albash, T. F. Rønnow, M. Troyer, and D. A. Lidar, “Probing for quantum speedup in spin-glass problems with planted solutions,” *Phys. Rev. A* **92**, 042325 (2015).
- ⁶²S. Boixo, V. N. Smelyanskiy, A. Shabani, S. V. Isakov, M. Dykman, V. S. Denchev, M. H. Amin, A. Y. Smirnov, M. Mohseni, and H. Neven, “Computational multiqubit tunnelling in programmable quantum annealers,” *Nat Commun* **7**, 10327 (2016).
- ⁶³S. Muthukrishnan, T. Albash, and D. A. Lidar, “Tunneling and Speedup in Quantum Optimization for Permutation-Symmetric Problems,” *Phys. Rev. X* **6**, 031010 (2016).
- ⁶⁴V. S. Denchev, S. Boixo, S. V. Isakov, N. Ding, R. Babbush, V. Smelyanskiy, J. Martinis, and H. Neven, “What is the Computational Value of Finite-Range Tunneling?” *Phys. Rev. X* **6**, 031015 (2016).
- ⁶⁵S. Mandrà, Z. Zhu, W. Wang, A. Perdomo-Ortiz, and H. G. Katzgraber, “Strengths and weaknesses of weak-strong cluster problems: A detailed overview of state-of-the-art classical heuristics versus quantum approaches,” *Phys. Rev. A* **94**, 022337 (2016).
- ⁶⁶S. Mandrà, Z. Zhu, and H. G. Katzgraber, “Exponentially Biased Ground-State Sampling of Quantum Annealing Machines with Transverse-Field Driving Hamiltonians,” *Phys. Rev. Lett.* **118**, 070502 (2017).
- ⁶⁷A. D. King, J. Raymond, T. Lanting, S. V. Isakov, M. Mohseni, G. Poulin-Lamarre, S. Ejtemaei, W. Bernoudy, I. Ozfidan, A. Y. Smirnov, M. Reis, F. Altomare, M. Babcock, C. Baron, A. J. Berkley, K. Boothby, P. I. Bunyk, H. Christiani, C. Enderud, B. Evert, R. Harris, E. Hoskinson, S. Huang, K. Jooya, A. Khodabandehlo, N. Ladizinsky, R. Li, P. A. Lott, A. J. R. MacDonald, D. Marsden, G. Marsden, T. Medina, R. Molavi, R. Neufeld, M. Norouzpour, T. Oh, I. Pavlov, I. Perminov, T. Prescott, C. Rich, Y. Sato, B. Sheldon, G. Sterling, L. J. Swenson, N. Tsai, M. H. Volkmann, J. D. Whittaker, W. Wilkinson, J. Yao, H. Neven, J. P. Hilton, E. Ladizinsky, M. W. Johnson, and M. H. Amin, “Scaling advantage over path-integral Monte Carlo in quantum simulation of geometrically frustrated magnets,” *Nat Commun* **12**, 1113 (2021).
- ⁶⁸R. Yaacoby, N. Schaar, L. Kellerhals, O. Raz, D. Hermelin, and R. Pugatch, “Comparison between a quantum annealer and a classical approximation algorithm for computing the ground state of an Ising spin glass,” *Phys. Rev. E* **105**, 035305 (2022).
- ⁶⁹A. D. King, S. Suzuki, J. Raymond, A. Zucca, T. Lanting, F. Altomare, A. J. Berkley, S. Ejtemaei, E. Hoskinson, S. Huang, E. Ladizinsky, A. J. R. MacDonald, G. Marsden, T. Oh, G. Poulin-Lamarre, M. Reis, C. Rich, Y. Sato, J. D. Whittaker, J. Yao, R. Harris, D. A. Lidar, H. Nishimori, and M. H. Amin, “Coherent quantum annealing in a programmable 2,000 qubit Ising chain,” *Nat. Phys.* **18**, 1324–1328 (2022).
- ⁷⁰H. Munoz-Bauza and D. Lidar, “Scaling Advantage in Approximate Optimization with Quantum Annealing,” *Phys. Rev. Lett.* **134**, 160601 (2025).
- ⁷¹A. Farhan, P. M. Derlet, A. Kleibert, A. Balan, R. V. Chopdekar, M. Wyss, L. Anghinolfi, F. Nolting, and L. J. Heyderman, “Exploring hyper-cubic energy landscapes in thermally active finite artificial spin-ice systems,” *Nature Physics* **9**, 375–382 (2013).
- ⁷²S. Roy and D. E. Logan, “The Fock-space landscape of many-body localisation,” *J. Phys.: Condens. Matter* **37**, 073003 (2025).
- ⁷³T. Lanting, A. D. King, B. Evert, and E. Hoskinson, “Experimental demonstration of perturbative anticrossing mitigation using nonuniform driver Hamiltonians,” *Phys. Rev. A* **96**, 042322 (2017).
- ⁷⁴Committee on Technical Assessment of the Feasibility and Implications of Quantum Computing, Computer Science and Telecommunications Board, Intelligence Community Studies Board, Division on Engineering and Physical Sciences, and National Academies of Sciences, Engineering, and Medicine, *Quantum Computing: Progress and Prospects*, edited by E. Grumbling and M. Horowitz (National Academies Press, 2019).
- ⁷⁵T. Graß, D. Raventós, B. Juliá-Díaz, C. Gogolin, and M. Lewenstein, “Quantum annealing for the number-partitioning problem using a tunable spin glass of ions,” *Nat Commun* **7**, 11524 (2016).
- ⁷⁶M. Qiao, Z. Cai, Y. Wang, B. Du, N. Jin, W. Chen, P. Wang, C. Luan, E. Gao, X. Sun, H. Tian, J. Zhang, and K. Kim, “Tunable quantum simulation of spin models with a two-dimensional ion crystal,” *Nat. Phys.* **20**, 623–630 (2024).
- ⁷⁷T. Inagaki, Y. Haribara, K. Igarashi, T. Sonobe, S. Tamate, T. Honjo, A. Marandi, P. L. McMahon, T. Umeki, K. Enbusu, O. Tadanaga, H. Takeuchi, K. Aihara, K.-i. Kawarabayashi, K. Inoue, S. Utsunomiya, and H. Takesue, “A coherent Ising machine for 2000-node optimization problems,” *Science* **354**, 603–606 (2016).
- ⁷⁸P. L. McMahon, A. Marandi, Y. Haribara, R. Hamerly, C. Langrock, S. Tamate, T. Inagaki, H. Takesue, S. Utsunomiya, K. Aihara, R. L. Byer, M. M. Fejer, H. Mabuchi, and Y. Yamamoto, “A fully programmable 100-spin coherent Ising machine with all-to-all connections,” *Science* **354**, 614–617 (2016).
- ⁷⁹F. Böhm, T. Inagaki, K. Inaba, T. Honjo, K. Enbusu, T. Umeki, R. Kasahara, and H. Takesue, “Understanding dynamics of coherent Ising machines through simulation of large-scale 2D Ising models,” *Nat Commun* **9**, 5020 (2018).
- ⁸⁰M. Babaeian, D. T. Nguyen, V. Demir, M. Akbulut, P.-A. Blanche, Y. Kaneda, S. Guha, M. A. Neifeld, and N. Peyghambarian, “A single shot coherent Ising machine based on a network of injection-locked multicore fiber lasers,” *Nat Commun* **10**, 3516 (2019).
- ⁸¹F. Böhm, G. Verschaffelt, and G. Van Der Sande, “A poor man’s coherent Ising machine based on opto-electronic feedback systems for solving optimization problems,” *Nat Commun* **10**, 3538 (2019).
- ⁸²R. Hamerly, T. Inagaki, P. L. McMahon, D. Venturelli, A. Marandi, T. Onodera, E. Ng, C. Langrock, K. Inaba, T. Honjo, K. Enbusu, T. Umeki, R. Kasahara, S. Utsunomiya, S. Kako, K.-i. Kawarabayashi, R. L. Byer, M. M. Fejer, H. Mabuchi, D. Englund, E. Rieffel, H. Takesue, and Y. Yamamoto, “Experimental investigation of performance differences between coherent Ising machines and a quantum annealer,” *Sci. Adv.* **5**, eaau0823 (2019).
- ⁸³T. Onodera, E. Ng, and P. L. McMahon, “A quantum annealer with fully programmable all-to-all coupling via Floquet engineering,” *npj Quantum Inf.* **6**, 48 (2020).
- ⁸⁴T. Honjo, T. Sonobe, K. Inaba, T. Inagaki, T. Ikuta, Y. Yamada, T. Kazama, K. Enbusu, T. Umeki, R. Kasahara, K.-i. Kawarabayashi, and H. Takesue, “100,000-spin coherent Ising machine,” *Sci. Adv.* **7**, eabh0952 (2021).
- ⁸⁵L. Luo, Z. Mi, J. Huang, and Z. Ruan, “Wavelength-division multiplexing optical Ising simulator enabling fully programmable spin couplings and external magnetic fields,” *Sci. Adv.* **9**, eadg6238 (2023).
- ⁸⁶D. Veraldi, D. Pierangeli, S. Gentilini, M. C. Strinati, J. Sakellariou, J. S. Cummins, A. Kamaletdinov, M. Syed, R. Z. Wang, N. G. Berloff, D. Karanikopoulos, P. G. Savvidis, and C. Conti, “Fully Programmable Spatial Photonic Ising Machine by Focal Plane Division,” *Phys. Rev. Lett.* **134**, 063802 (2025).
- ⁸⁷V. Torggler, S. Krämer, and H. Ritsch, “Quantum annealing with ultracold atoms in a multimode optical resonator,” *Phys. Rev. A* **95**, 032310 (2017).
- ⁸⁸R. M. Kroese, B. P. Marsh, D. Atri Schuller, H. S. Hunt, A. N. Bourzutschky, M. Winer, S. Gopalakrishnan, J. Keeling, and B. L. Lev, “Directly observing replica symmetry breaking in a vector quantum-optical spin glass,” *Science* **389**, 1122–1126 (2025).
- ⁸⁹B. P. Marsh, D. A. Schuller, Y. Ji, H. S. Hunt, G. Z. Socolof, D. P. Bowman, J. Keeling, and B. L. Lev, “Multimode Cavity QED Ising Spin Glass,” *Phys. Rev. Lett.* **135**, 160403 (2025).
- ⁹⁰A. W. Glaetzle, R. M. W. Van Bijnen, P. Zoller, and W. Lechner, “A coherent quantum annealer with Rydberg atoms,” *Nat Commun* **8**, 15813 (2017).
- ⁹¹X. Qiu, P. Zoller, and X. Li, “Programmable Quantum Annealing Architectures with Ising Quantum Wires,” *PRX Quantum* **1**, 020311 (2020).
- ⁹²A. Lucas, “Ising formulations of many NP problems,” *Front. Physics* **2**, 1–14 (2014).
- ⁹³R. K. Nath, H. Thapliyal, and T. S. Humble, “A Review of Machine Learning Classification Using Quantum Annealing for Real-World Applications,” *SN COMPUT. SCI.* **2**, 365 (2021).
- ⁹⁴H. Salloum, R. Lukin, and M. Mazzara, “Quantum Computing in Drug Discovery: A Review of Quantum Annealing and Gate-Based Approaches,” in *International Conference on Computational Optimization* (2024).
- ⁹⁵M. Q. Mohammed, H. Meeß, and M. Otte, “Review of the application of quantum annealing-related technologies in transportation optimization,” *Quantum Inf Process* **24**, 296 (2025).
- ⁹⁶Y. Horie and Y. Kawaguchi, “A comprehensive exploration of interaction networks reveals a connection between entanglement and network structure,” (2025).
- ⁹⁷R. J. Glauber, “Time-Dependent Statistics of the Ising Model,” *J. Math. Phys.* **4**, 294–307 (1963).
- ⁹⁸P. W. Anderson, “Absence of Diffusion in Certain Random Lattices,” *Phys. Rev.* **109**, 1492–1505 (1958).
- ⁹⁹Y. Horie and S. Fujishiro, “Orthogonal projections of hypercubes,” *Phys. Rev. E* **112**, 045304 (2025).
- ¹⁰⁰Y. Horie, “The data and code for paper ‘TBA’,” Zenodo (2025).
- ¹⁰¹G. van Rossum and F. L. Drake, *The Python Language Reference*, release 3.0.1 [repr.] ed., Python Documentation Manual / Guido van Rossum; Fred L. Drake [Ed.] No. Pt. 2 (Python Software Foundation, 2010).
- ¹⁰²J. D. Hunter, “Matplotlib: A 2D Graphics Environment,” *Comput. Sci. Eng.* **9**, 90–95 (2007).
- ¹⁰³A. A. Hagberg, D. A. Schult, and P. J. Swart, “Exploring Network Structure, Dynamics, and Function using NetworkX,” in *Proc. 7th Python Sci. Conf.* (2008) pp. 11–15.
- ¹⁰⁴S. K. Lam, A. Pitrou, and S. Seibert, “Numba: A LLVM-based Python JIT compiler,” in *Proc. Second Workshop LLVM Compil. Infrastruct. HPC*, LLVM ’15 (ACM, 2015) pp. 1–6.
- ¹⁰⁵C. R. Harris, K. J. Millman, S. J. Van Der Walt, R. Gommers, P. Virtanen, D. Cournapeau, E. Wieser, J. Taylor, S. Berg, N. J. Smith, R. Kern, M. Picus,

- S. Hoyer, M. H. Van Kerkwijk, M. Brett, A. Haldane, J. F. Del Río, M. Wiebe, P. Peterson, P. Gérard-Marchant, K. Sheppard, T. Reddy, W. Weckesser, H. Abbasi, C. Gohlke, and T. E. Oliphant, “Array programming with NumPy,” *Nature* **585**, 357–362 (2020).
- ¹⁰⁶J. Johansson, P. Nation, and F. Nori, “QuTiP: An open-source Python framework for the dynamics of open quantum systems,” *Comput. Phys. Commun.* **183**, 1760–1772 (2012).
- ¹⁰⁷J. Johansson, P. Nation, and F. Nori, “QuTiP 2: A Python framework for the dynamics of open quantum systems,” *Comput. Phys. Commun.* **184**, 1234–1240 (2013).
- ¹⁰⁸N. Lambert, E. Giguère, P. Menczel, B. Li, P. Hopf, G. Suárez, M. Gali, J. Lishman, R. Gadhvi, R. Agarwal, A. Galicia, N. Shammah, P. Nation, J. R. Johansson, S. Ahmed, S. Cross, A. Pitchford, and F. Nori, “QuTiP 5: The Quantum Toolbox in Python,” [arXiv.org abs/2412.04705](https://arxiv.org/abs/2412.04705) (2024), 10.48550/arXiv.2412.04705.
- ¹⁰⁹P. Virtanen, R. Gommers, T. E. Oliphant, M. Haberland, T. Reddy, D. Cournapeau, E. Burovski, P. Peterson, W. Weckesser, J. Bright, S. J. Van Der Walt, M. Brett, J. Wilson, K. J. Millman, N. Mayorov, A. R. J. Nelson, E. Jones, R. Kern, E. Larson, C. J. Carey, İ. Polat, Y. Feng, E. W. Moore, J. VanderPlas, D. Laxalde, J. Perktold, R. Cimrman, I. Henriksen, E. A. Quintero, C. R. Harris, A. M. Archibald, A. H. Ribeiro, F. Pedregosa, P. Van Mulbregt, SciPy 1.0 Contributors, A. Vijaykumar, A. P. Bardelli, A. Rothberg, A. Hilboll, A. Kloeckner, A. Scopatz, A. Lee, A. Rokem, C. N. Woods, C. Fulton, C. Masson, C. Häggström, C. Fitzgerald, D. A. Nicholson, D. R. Hagen, D. V. Pasechnik, E. Olivetti, E. Martin, E. Wieser, F. Silva, F. Lenders, F. Wilhelm, G. Young, G. A. Price, G.-L. Ingold, G. E. Allen, G. R. Lee, H. Audren, I. Probst, J. P. Dietrich, J. Silterra, J. T. Webber, J. Slavić, J. Nothman, J. Buchner, J. Kulick, J. L. Schönberger, J. V. De Miranda Cardoso, J. Reimer, J. Harrington, J. L. C. Rodríguez, J. Nunez-Iglesias, J. Kuczynski, K. Tritz, M. Thoma, M. Newville, M. Kümmeler, M. Bolingbroke, M. Tartre, M. Pak, N. J. Smith, N. Nowaczyk, N. Shebanov, O. Pavlyk, P. A. Brodtkorb, P. Lee, R. T. McGibbon, R. Feldbauer, S. Lewis, S. Tygier, S. Sievert, S. Vigna, S. Peterson, S. More, T. Pudlik, T. Oshima, T. J. Pingel, T. P. Robitaille, T. Spura, T. R. Jones, T. Cera, T. Leslie, T. Zito, T. Krauss, U. Upadhyay, Y. O. Halchenko, and Y. Vázquez-Baeza, “SciPy 1.0: Fundamental algorithms for scientific computing in Python,” *Nat. Methods* **17**, 261–272 (2020).
- ¹¹⁰P. Kovesi, “Good Colour Maps: How to Design Them,” [arXiv](https://arxiv.org/abs/1509.03700) (2015), 10.48550/arXiv.1509.03700.

METHODS

Generation of all possible interaction networks

To generate all possible interaction networks of N spins, we perform the brute force search over all possible combinations of the interaction matrix $\mathbf{J} \in \{+J/N, -J/N, 0\}^{N \times N}$, then remove the non-connected and isomorphic networks. The number of all possible interaction networks is available in Method section of ref.⁹⁶.

Ising spin system and annealing dynamics

Following ref.⁷, we investigate the thermal and QA of the Ising spin system on various networks. See the detailed comparison between TA and QA in ref.¹⁰ For TA, we consider the classical Ising spin system defined by Hamiltonian $H(\mathbf{s}) \in \mathbb{R}$,

$$H(\mathbf{s}) := -\frac{1}{2} \sum_{i=1}^N \sum_{j=1}^N s_i J_{i,j} s_j - \sum_{i=1}^N s_i h_i = -\frac{1}{2} \mathbf{s}^\top \mathbf{J} \mathbf{s} - \mathbf{s}^\top \mathbf{h}, \quad (1)$$

where $\mathbf{s} := [s_1 \ \cdots \ s_N]^\top \in \{\uparrow := +1, \downarrow := -1\}^N$ is a state vector of N Ising spins, $\mathbf{J} \in \{+J/N, -J/N, 0\}^{N \times N}$ is the interaction matrix with elements $J_{i,j}$, and $\mathbf{h} := [h_1 \ \cdots \ h_N]^\top \in \mathbb{R}^N$ is the longitudinal field vector. Note that we set $J = 1$ throughout this work and factor $1/N$ is introduced for extensive energy scaling (Kac scaling). The state space is hypercube and each vertex is associated with a state vector \mathbf{s} . The state space is called hypercubic energy landscape⁷¹.

Assuming Markov process, and that the system is in contact with a time-dependent thermal bath at temperature $T(t) = \frac{1}{\beta(t)} \in \mathbb{R}_{>0}$, the probability of finding the system in the state \mathbf{s} at time t , $p(\mathbf{s}; t) \in [0, 1]$, is governed by the master equation

$$\frac{d}{dt} \mathbf{p}(t) = \mathbf{W}(t) \mathbf{p}(t). \quad (2)$$

Here, $\mathbf{p}(t) := [\cdots \ p(\mathbf{s}; t) \ \cdots]^\top \in [0, 1]^{2^N}$ is the probability vector, which is the statistical state of the system, and $\mathbf{W}(t) \in \mathbb{R}_{>0}^{2^N \times 2^N}$ is the transition rate matrix with elements $W_{\mathbf{s}, \mathbf{s}'}(t)$. We define the transition rate from state \mathbf{s}' to \mathbf{s} as Glauber type⁹⁷,

$$W_{\mathbf{s}, \mathbf{s}'}(t) := \begin{cases} w(\mathbf{s}, \mathbf{s}'; t) & \text{if } \mathbf{s}' = \mathbf{F}_k \mathbf{s} \\ -\sum_{\mathbf{s}'} w(\mathbf{s}', \mathbf{s}; t) & \text{if } \mathbf{s}' = \mathbf{s} \\ 0 & \text{otherwise} \end{cases}, \quad (3)$$

where

$$w(\mathbf{s}, \mathbf{s}'; t) := \frac{1}{1 + \exp(\beta(t)[H(\mathbf{s}) - H(\mathbf{s}')])} \quad (4)$$

and the spin flip matrix is defined as $\mathbf{F}_k := \mathbf{I} - 2\mathbf{e}_k \mathbf{e}_k^\top$, where $\mathbf{I} := \text{diag}(\mathbf{1})$ is the identity matrix, and \mathbf{e}_k is the k th standard basis vector in \mathbb{R}^N . The k th element of the state vector \mathbf{s} is flipped by multiplying \mathbf{F}_k as $\mathbf{F}_k \mathbf{s} = [s_1 \ \cdots \ -s_k \ \cdots \ s_N]^\top$.

For QA, we consider the quantum Ising model (or transverse-field Ising model) defined by time-dependent Hamiltonian,

$$\hat{H}(t) := \underbrace{-\frac{1}{2} \sum_{i=1}^N \sum_{j=1}^N J_{i,j} \hat{Z}_i \hat{Z}_j}_{=: \hat{H}_z} - \underbrace{\sum_{i=1}^N h_i \hat{Z}_i - \Gamma(t) \sum_{i=1}^N \hat{X}_i}_{=: \hat{H}_x(t)}, \quad (5)$$

where \hat{X}_i and \hat{Z}_i are the Pauli X and Z operators acting on the i th spin respectively, i.e.,

$$\hat{X}_i := \bigotimes_{j=1}^N \begin{cases} \hat{\sigma}_x & \text{if } j = i \\ \mathbf{I} & \text{otherwise} \end{cases}, \quad (6)$$

and

$$\hat{Z}_i := \bigotimes_{j=1}^N \begin{cases} \hat{\sigma}_z & \text{if } j = i \\ \mathbf{I} & \text{otherwise} \end{cases}. \quad (7)$$

Note that $\hat{\sigma}_x := \begin{bmatrix} 0 & 1 \\ 1 & 0 \end{bmatrix}$ and $\hat{\sigma}_z := \begin{bmatrix} 1 & 0 \\ 0 & -1 \end{bmatrix}$. Transverse field strength at time t is given as $\Gamma(t) \in \mathbb{R}_{>0}$. The time independent term \hat{H}_z is called the problem Hamiltonian, as its ground state encodes the solution of the optimization problem. The time-dependent term $\hat{H}_x(t)$ is called the driver Hamiltonian, which introduces quantum fluctuations to the system.

The time evolution of the wave function $|\psi(t)\rangle$ is governed by the Schrödinger equation:

$$\frac{d}{dt} |\psi(t)\rangle = -i\hat{H}(t) |\psi(t)\rangle. \quad (8)$$

The analogy between thermal and QA is highlighted by expressing the Hamiltonian of the transverse-field Ising model in the Fock basis. The Hamiltonian is decomposed into time-independent diagonal part \hat{H}_z and time-dependent off-diagonal part $\hat{H}_x(t)$. Using Fock bases, $\{|s\rangle\}$, the Hamiltonian $\hat{H}(t)$ are rewritten as:

$$\begin{aligned} \hat{H}(t) = & \sum_{\mathbf{s}} H(\mathbf{s}) |s\rangle \langle s| \\ & + \sum_{\mathbf{s}} \sum_{k=1}^N K(\mathbf{s}, \mathbf{F}_k \mathbf{s}; t) |s\rangle \langle \mathbf{F}_k \mathbf{s}|. \end{aligned} \quad (9)$$

Here, Fock basis is defined as $|s\rangle := \bigotimes_{i=1}^N |s_i\rangle_i$, which is the eigenstate of \hat{H}_z . The diagonal element $H(\mathbf{s})$ is given as the energy of the classical Ising spin system of equation (1). The off-diagonal element is given as $K(\mathbf{s}, \mathbf{F}_k \mathbf{s}; t) := -\Gamma(t)$. With this notation, the Hamiltonian can be considered as the Anderson model of localization^{15,72,98}, where the particle hops from sites $|\mathbf{F}_k \mathbf{s}\rangle$ to $|s\rangle$ with on-site potential $H(\mathbf{s})$ and hopping amplitude $K(\mathbf{s}, \mathbf{F}_k \mathbf{s}; t)$.

We consider three types of annealing schedules⁷: reciprocal, reciprocal square root, and reciprocal logarithm schedules. Those are given as follows,

$$T(t) = \Gamma(t) = \begin{cases} c/t & \text{(reciprocal)} \\ c/\sqrt{t} & \text{(reciprocal square root)} \\ c/\ln(1+t) & \text{(reciprocal logarithm)} \end{cases}. \quad (10)$$

We set the constant $c = 3$ throughout this work. In both annealing methods, the system is initialized in the $t \rightarrow 0$ limit of the corresponding annealing schedule. For TA, the initial statistical state is the high-temperature limit, $p(\mathbf{s}; 0) \approx 1/2^N$, $\forall \mathbf{s}$, and for QA, the initial wave function is the ground state of $\hat{H}_x(0)$, $|\psi(0)\rangle \approx \bigotimes_{i=1}^N \frac{1}{\sqrt{2}}(|\uparrow\rangle_i + |\downarrow\rangle_i)$. In both TA and QA, the state of the system converge to the ground state of $H(\mathbf{s})$ or \hat{H}_z at the end of annealing process, $t \rightarrow \infty$, i.e., the statistical state is expected to converge the Kronecker delta function, $p(\mathbf{s}; \infty) \sim \delta_{\mathbf{s}, \mathbf{s}_g}$ for TA, and the wave function is expected to converge the Fock state, $|\psi(\infty)\rangle \sim |s_g\rangle$ for QA, where s_g is the ground state of equation (1), and $g := \arg \min_{\mu} (H(s_{\mu}))$ is index specifying the ground state.

The performance of annealing is evaluated by the success rate, which corresponds to the probability of finding the ground state⁷. For TA, the success rate is simply given by $p_{\text{TA}}(t) := p(s_g; t)$, and for QA, it is given by $p_{\text{QA}}(t) := |\langle s_g | \psi(t) \rangle|^2$. It is useful to introduce the annealing success rate of adiabatic process⁷, which is defined as the probability of finding the ground state in the adiabatic limit of each annealing schedule, i.e., in the limit of infinitely slow annealing. For TA, this is given by the Boltzmann distribution at temperature $T(t)$, $p_{\text{ATA}}(t) = \pi(s_g; t) := \frac{1}{Z(t)} \exp(-\beta(t)H(s_g))$ with partition function $Z(t) := \sum_s \exp(-\beta(t)H(s))$, and for QA, this is given by, $p_{\text{AQA}}(t) := |\langle s_g | \phi(t) \rangle|^2$, where $|\phi(t)\rangle$ is the instantaneous ground state of $\hat{\mathcal{H}}(t)$. Note that the eigenvector of the transition rate matrix [equation (3)] with zero eigenvalue, $\mathbf{W}(t)\mathbf{p}_0(t) = 0\mathbf{p}_0(t)$, is proportional to the Boltzmann distribution at temperature $T(t)$, $\mathbf{p}_0(t) \propto \boldsymbol{\pi}(t)$, where $\boldsymbol{\pi}(t) := [\cdots \pi(s; t) \cdots]^\top$.

Thermal and quantum probability flux

Probability flux between states characterizes the dynamics of both thermal and QA. For TA, the master equation is rewritten with the thermal probability flux as

$$\frac{d}{dt}p(s; t) = \sum_{s'} [w(s, s'; t)p(s'; t) - w(s', s; t)p(s; t)] \quad (11)$$

$$= \sum_{s'} \mathcal{J}_{\text{T}}(s, s'; t). \quad (12)$$

Here, thermal probability flux is defined as

$$\mathcal{J}_{\text{T}}(s, s'; t) := w(s, s'; t)p(s'; t) - w(s', s; t)p(s; t), \quad (13)$$

which is the difference between the forward and backward joint transition rates. By integrating both sides of Eq. (12) from $t = 0$ to $t = \infty$, we have

$$p(s; \infty) - p(s; 0) = \sum_{s'} \Delta \mathcal{J}_{\text{T}}(s, s'), \quad (14)$$

where

$$\Delta \mathcal{J}_{\text{T}}(s, s') := \int_0^\infty dt \mathcal{J}_{\text{T}}(s, s'; t) \quad (15)$$

is the time-integrated thermal probability flux from state s' to s .

Quantum probability flux between Fock states is derived as below. The wave function $|\psi(t)\rangle$ is expanded in the Fock basis $|s\rangle$ as

$$|\psi(t)\rangle = \left(\sum_s |s\rangle \langle s| \right) |\psi(t)\rangle = \sum_s c(s; t) |s\rangle, \quad (16)$$

where $c(s; t) := \langle s | \psi(t) \rangle \in \mathbb{C}$ is the probability amplitude of the Fock state $|s\rangle$ at time t . The probability of finding the system in the Fock state $|s\rangle$ is $|c(s; t)|^2 = c^*(s; t)c(s; t) \in [0, 1]$. Using the Schrödinger equation of equation (8), we have $\sum_{s'} |s'\rangle \frac{dc(s', t)}{dt} = \sum_{s'} [-i\hat{\mathcal{H}}(t)] |s'\rangle c(s'; t)$. Multiplying $\langle s |$ from the left side, we obtain

$$\frac{dc(s; t)}{dt} = \sum_{s'} \langle s | [-i\hat{\mathcal{H}}(t)] |s'\rangle c(s'; t). \quad (17)$$

Then, the time evolution of $|c(s; t)|^2$ is given by

$$\begin{aligned} \frac{d}{dt} |c(s; t)|^2 &= \frac{dc(s; t)^*}{dt} c(s; t) + c(s; t)^* \frac{dc(s; t)}{dt} \\ &= \sum_{s'} [-c^*(s'; t) \langle s' | [-i\hat{\mathcal{H}}(t)] |s\rangle c(s; t) \\ &\quad + c^*(s; t) \langle s | [-i\hat{\mathcal{H}}(t)] |s'\rangle c(s'; t)] \end{aligned} \quad (18)$$

$$= \sum_{s'} \mathcal{J}_{\text{Q}}(s, s'; t), \quad (19)$$

where we define the quantum probability flux from Fock state $|s'\rangle$ to $|s\rangle$ as

$$\mathcal{J}_{\text{Q}}(s, s'; t) := c^*(s; t) \langle s | [-i\hat{\mathcal{H}}(t)] |s'\rangle c(s'; t) - c^*(s'; t) \langle s' | [-i\hat{\mathcal{H}}(t)] |s\rangle c(s; t) \quad (20)$$

$$= 2 \operatorname{Re}[c^*(s; t) \langle s | [-i\hat{\mathcal{H}}(t)] |s'\rangle c(s'; t)]. \quad (21)$$

Similarly to the thermal case, by integrating both sides of equation (19) from $t = 0$ to $t = \infty$, we have

$$|c(s; \infty)|^2 - |c(s; 0)|^2 = \sum_{s'} \Delta \mathcal{J}_{\text{Q}}(s, s'), \quad (22)$$

where

$$\Delta \mathcal{J}_{\text{Q}}(s, s') := \int_0^\infty dt \mathcal{J}_{\text{Q}}(s, s'; t) \quad (23)$$

is the time-integrated quantum probability flux from Fock state $|s'\rangle$ to $|s\rangle$.

Probability flux diagram

To visualize the probability fluxes of TA and QA, we introduce the probability flux diagram. The diagram is a directed graph, where each node represents a hypercubic state s , and each directed edge from node s' to s represents the (time-integrated) probability flux. Note that each directed edge corresponds to a hypercubic edge which is a state transition involving a single spin flip. The state space is called hypercubic energy landscape⁷¹ for thermal-fluctuation-driven system, and is called Fock state landscape⁷² for quantum fluctuation-driven system.

The diagram is projected by principal component analysis (PCA), which reflects underlying structure of the interaction network⁹⁹. For each node s , we calculate the cumulative probability,

$$\varrho_{\text{T}}(s) := A \int_0^\infty dt p(s; t), \quad (24)$$

or

$$\varrho_{\text{Q}}(s) := A \int_0^\infty dt |c(s; t)|^2, \quad (25)$$

where $A := 1/\sum_s \varrho(s)$ is the normalization constant. Then, we calculate the covariance matrix,

$$\Sigma := \langle (s - \langle s \rangle_{\varrho})(s - \langle s \rangle_{\varrho})^\top \rangle_{\varrho}. \quad (26)$$

Here, the expectation with respect to ϱ is indicated as subscript. Using the eigenvectors, \mathbf{u}_1 and \mathbf{u}_2 , of the covariance matrix which have the first and the second-largest eigenvalues, λ_1 and λ_2 , we project each node s onto two-dimensional plane,

$$\mathbf{r}(s) := \begin{bmatrix} \mathbf{u}_1^\top s \\ \mathbf{u}_2^\top s \end{bmatrix}. \quad (27)$$

The directed edges are drawn between the projected nodes according to the (time-integrated) probability fluxes.

Data availability

Previously generated data⁹⁶ are used in this study. All data are available online from Zenodo¹⁰⁰. <https://doi.org/10.5281/zenodo.0000000>.

Code availability

Calculations and visualizations of this work were performed using open-source Python¹⁰¹ libraries: Matplotlib¹⁰², NetworkX¹⁰³, Numba¹⁰⁴, NumPy¹⁰⁵, QuTiP^{106–108}, and SciPy¹⁰⁹. The colour map of some figures are generated by ColorCET¹¹⁰. All code are available online from Zenodo¹⁰⁰. <https://doi.org/10.5281/zenodo.0000000>.

Acknowledgements Y.H. thanks Andrew D. King for fruitful discussions on ref.¹⁸. Y.H. is supported by SPRING Grant No. JPMJSP2125 “THERS Make New Standards Program for the Next Generation Researchers” of the Japan Science and Technology Agency.

Author contributions Y.H. performed conceptualization, data curation, formal analysis, investigation, software development, validation, and visualization. Y.H. and Y.K. developed methodology and acquired funding. Y.H. administered the project, and Y.K. supervised the work. Y.H. wrote the original draft, and Y.H. and Y.K. reviewed and edited the manuscript.

Competing interests All authors declare no competing interests.

Additional information

Supplementary information The online version contains supplementary material.

Correspondence and requests for materials should be addressed to Y.H.